Electronic Supplementary Materials

For https://doi.org/10.1631/jzus.A2400427

Probabilistic analysis of settlement characteristics induced by shield tunnelling in sandy cobble strata considering the spatial variability

Fan WANG[1], Pengfei LI[2✉], Xiuli DU[2], Jianjun MA[1], Lin WANG[1]

[1]*School of Civil Engineering and Architecture, Henan University of Science and Technology, Luoyang 471023, China*

[2]*Key Laboratory of Urban Security and Disaster Engineering, Ministry of Education, Beijing University of Technology, Beijing 100124, China*

Section S1 Parameter calibration for strain-hardening model

Wang et al. (2024) developed the stochastic structural models of sandy cobble soil with different *VBP*s considering the random distribution of cobbles. Numerical tests under biaxial compression were performed to obtain the stress-strain curves for different *VBP*s. Subsequently, the material parameters in the Hardening-Soil model were calibrated based on these stress-strain curves. The densities ρ were calculated through the volumetric weighting of cobbles and soil matrix (Du et al., 2019). p^{ref} was commonly assumed as the standard atmospheric pressure (i.e. 100kPa). A typical value of 0.2 was commonly adopted for v_{ur}. The value of R_f was fixed at 0.99. Due to the low clay content in sandy cobble soil, the soil was assumed to be cohesionless. The calibration of φ was consistent with that of the Mohr-Coulomb model. The parameter ψ was adjusted through trial and error to ensure the stress-strain curve evolves in a stable, continuous manner, devoid of significant oscillations. E_{50}^{ref} and m were determined through fitting the linear form of the hyperbolic relationship between the deviatoric stress and axial strain. E_{50}^{ref} and E_{oed}^{ref} control the magnitude of plastic strains that originate from the yield surface and yield cap, respectively (Schanz et al., 1999). E_{ur}^{ref} typically employs a value within the range of 3 to 5 times E_{50}^{ref} for most soils. It is generally assumed that these three parameters follow a relationship, expressed as $E_{ur}^{ref} = 3E_{50}^{ref}$ and $E_{oed}^{ref} = E_{50}^{ref}$. The detail process of parameter calibration refers to Wang et al. (2024).

Table S1 Material parameters for different *VBP*s

VBP/%	ρ / kg·m^{-3}	E_{50}^{ref} / MPa	E_{oed}^{ref} / MPa	E_{ur}^{ref} / MPa	p^{ref} / kPa	v_{ur}	m	R_f	c / kPa	φ / °	ψ / °
30	2210	25	25	75	100	0.2	0.776	0.99	0	27.57	10
50	2350	40	40	120	100	0.2	0.736	0.99	0	34.95	20
70	2490	70	70	210	100	0.2	0.5	0.99	0	49	30

Note: The meaning of each symbol in the table from left to right is the volumetric block proportion, density, reference secant modulus, reference tangent modulus for primary oedometer loading, reference Young's modulus for unloading and reloading, reference stress, Poisson's ratio for uploading-reloading, amount of stress dependency, failure ratio, cohesion, friction angle, dilation angle, respectively.

Section S2 Discretization of random field using the Karhunen-Loève series expansion

For practical application, only a finite number of terms (M) are enough to satisfy the minimum mean square approximation error (Huang et al., 2001). The Karhunen-Loève series expansion for the two-dimensional random field X can be expressed as follows:

$$H_X(x,y) = \mu_X + \sum_{n=1}^{M} \sigma_X \sqrt{\lambda_n} f_n(x,y) \xi_{X,n} \tag{S1}$$

where (x, y) is the coordinate of a point in the two-dimensional computational domain. μ_X and σ_X are the mean value and standard deviation, respectively. λ_n and $f_n(x, y)$ represent the eigenvalue and eigenfunction of the autocorrelation function $\rho_X(x, y)$, respectively. $\xi_{X,n}$ is a set of orthogonal and uncorrelated random variables with zero mean value and unit variance. The value of M depends on the desired accuracy and the autocorrelation function. According to the existing researches (Laloy et al., 2013; Jiang et al., 2014), the number M can be measured by the ratio of the expected energy (i.e., $\varepsilon = \sum_{n=1}^{M} \lambda_n / \sum_{n=1}^{\infty} \lambda_n$). When $\varepsilon \geq 95\%$, the desired accuracy is achieved.

The series expansion of the lognormal random field can be denoted as follows:

$$H_X^{LN}(x,y) = \exp\left[\mu_{\ln X} + \sum_{j=1}^{M} \sigma_{\ln X} \sqrt{\lambda_j} f_j(x,y) \xi_{X,j} \right] \tag{S2}$$

where $\mu_{\ln X}$ and $\sigma_{\ln X}$ are the mean value and standard deviation of Gaussian random field ln$X$, respectively. The relationship between X and ln$X$ is expressed by:

$$\begin{cases} \mu_{\ln X} = \ln \mu_X - \dfrac{\sigma_{\ln X}^2}{2} \\ \sigma_{\ln X} = \sqrt{\ln\left[1 + (\sigma_X / \mu_X)^2\right]} \end{cases} \tag{S3}$$

Section S3 Representation in FLAC3D of random field modeling for E50ref and φ

Fig. S1 displays the representation in FLAC^{3D} of random field modeling for E_{50}^{ref} and φ when VBP =50%, respectively. The input parameters are as follows: μ_E = 40 MPa, μ_φ = 34.95°, COV_E = COV_φ = 0.1, $\rho_{\varphi,E}$ = 0, δ_h = 40 m, and δ_v = 4 m. It is found that the random fields generated by the Gaussian autocorrelation function behave good stationarity and continuity.

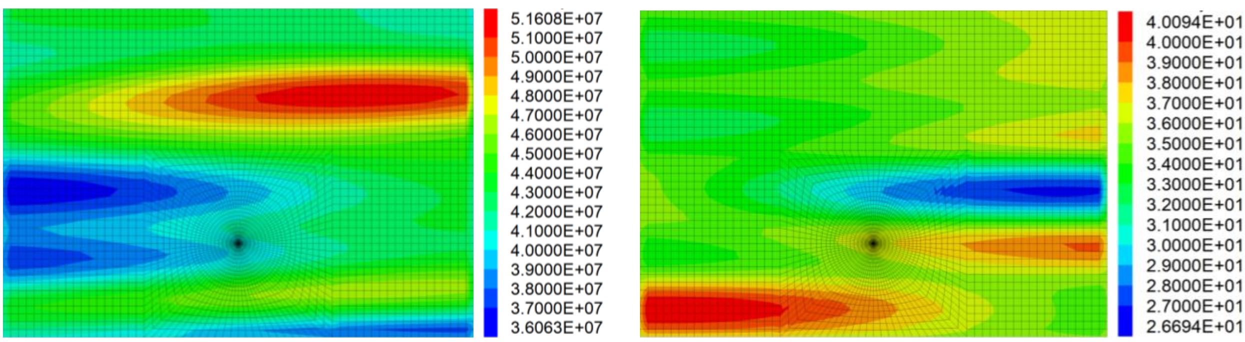

(a) (b)

Fig. S1 Representation in FLAC^{3D} of random field modeling: (a) E_{50}^{ref} (unit: Pa); (b) φ (unit: degree)

Section S4 Results and comparisons of surface settlement

Fig. S2 compares the profiles of surface settlement trough obtained by stochastic and deterministic analyses. $S(x)$ represents the surface settlement at the point $(x, 0)$. It can be seen that the stochastic results fluctuate randomly above and below the deterministic results. All the stochastic analysis results of surface settlement decrease with the increase of *VBP* and the decrease of η_t, which is consistent with the deterministic analysis results. Furthermore, the higher the *VBP* or the greater the η_t, the higher the dispersion of stochastic analysis results.

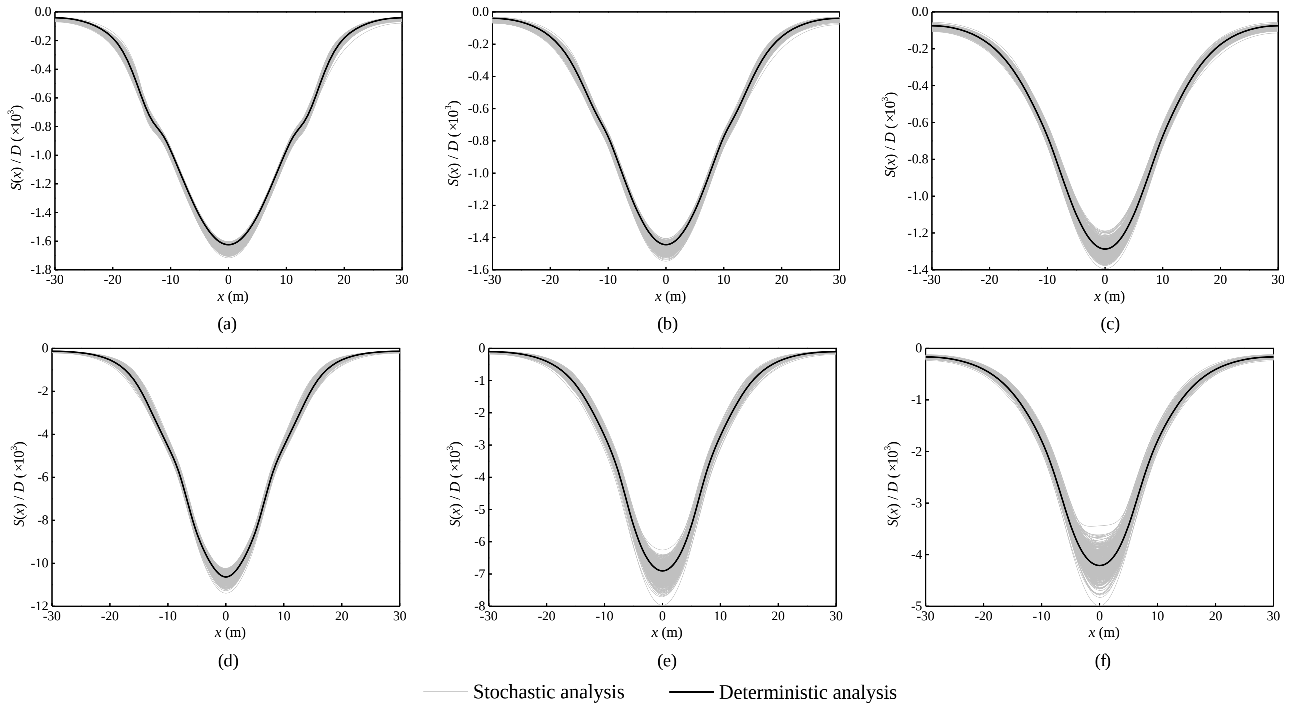

Fig. S2 Comparison of the profiles of surface settlement trough between stochastic and deterministic analyses: (a)*VBP* = 30%, η_t = 0.5%; (b) *VBP* = 50%, η_t = 0.5%; (c) *VBP* = 70%, η_t = 0.5%; (d) *VBP* = 30%, η_t = 4.0%; (e) *VBP* = 50%, η_t = 4.0%; (f) *VBP* = 70%, η_t = 4.0%

Section S5 Volumetric deformation modes of sandy cobble soil

Wang et al. (2024) defined expressions of $\eta_s(z)/\eta_t$ and $\eta_s'(z)$ (i.e., the first derivative of $\eta_s(z)$) to determine the overall and localized responses of volumetric deformation of the soil at a certain depth z. Note that the overall response of volumetric deformation refers to the cumulative volumetric deformation of the soil beneath the given depth z, while the localized response refers to the volumetric deformation of an infinitesimal soil layer with the thickness of dz at the given depth z. The criterions of $\eta_s(z)/\eta_t > 1.0$, $\eta_s(z)/\eta_t = 1.0$, and $\eta_s(z)/\eta_t < 1.0$ correspond to the contractive, constant and dilative overall volumetric deformation responses at the given depth, respectively. The criterions of $\eta_s'(z) > 0$, $\eta_s'(z) = 0$, and $\eta_s'(z) < 0$ correspond to the dilative, constant and contractive localized volumetric deformation responses at the given depth, respectively. According to the localized response of volumetric deformation, Wang et al. (2024) proposed three volumetric deformation modes of sandy cobble soil, as shown in Fig. S3. The detail description about the volumetric deformation modes refers to Wang et al. (2024).

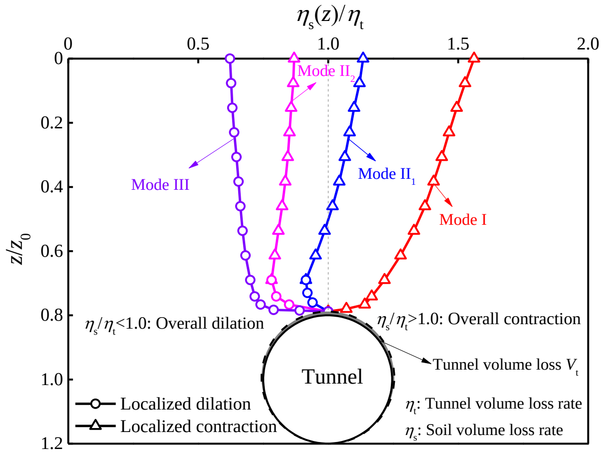

Fig. S3 Three volumetric deformation modes of sandy cobble soil

Section S6 Variation of the mean of stochastic analysis results with depth

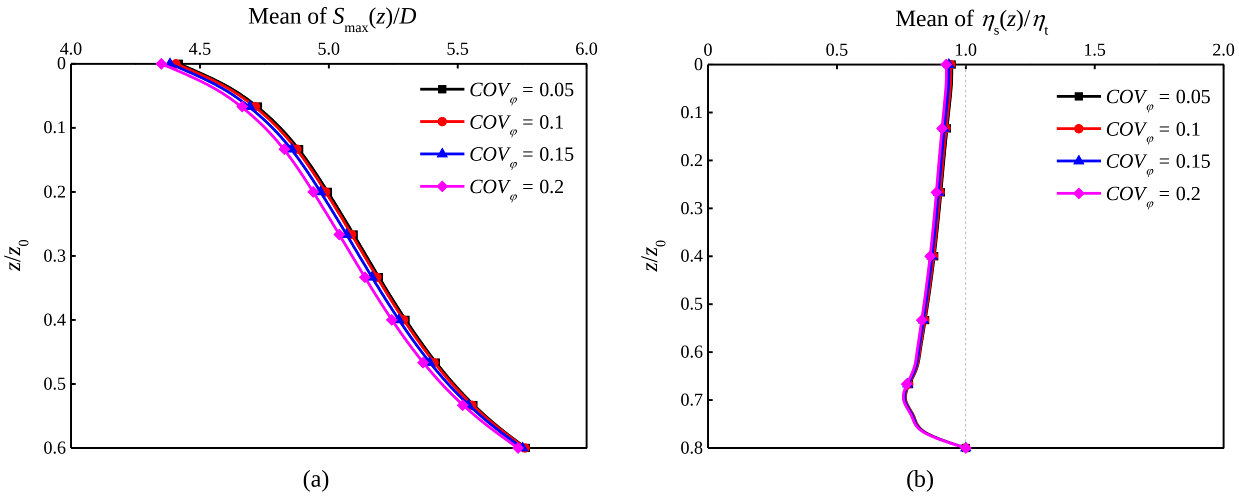

Fig. S4 Mean of stochastic analysis results under different COV_{φ}: (a) Normalized subsurface maximum settlement; (b) Normalized subsurface soil volume loss rate

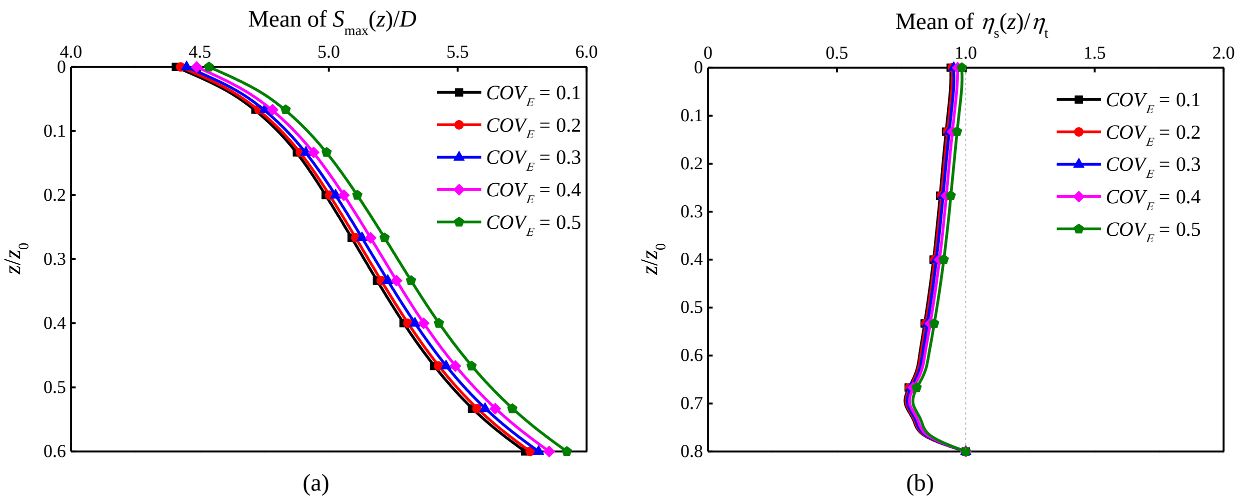

Fig. S5 Mean of stochastic analysis results under different COV_E: (a) Normalized subsurface maximum settlement; (b) Normalized subsurface soil volume loss rate

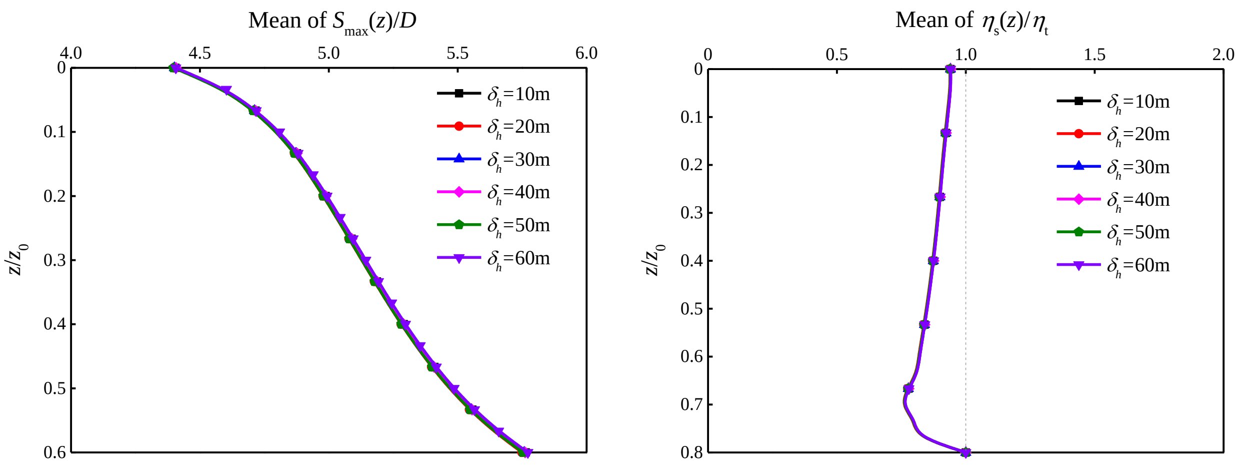

(a) (b)

Fig. S6 Mean of stochastic analysis results under different δ_h: (a) Normalized subsurface maximum settlement; (b) Normalized subsurface soil volume loss rate

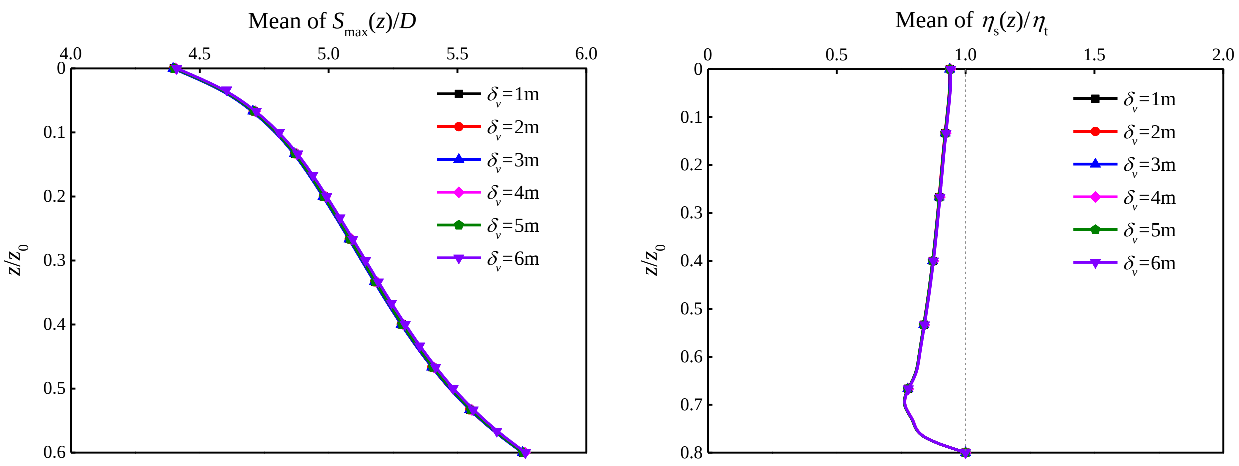

(a) (b)

Fig. S7 Mean of stochastic analysis results under different δ_v: (a) Normalized subsurface maximum settlement; (b) Normalized subsurface soil volume loss rate

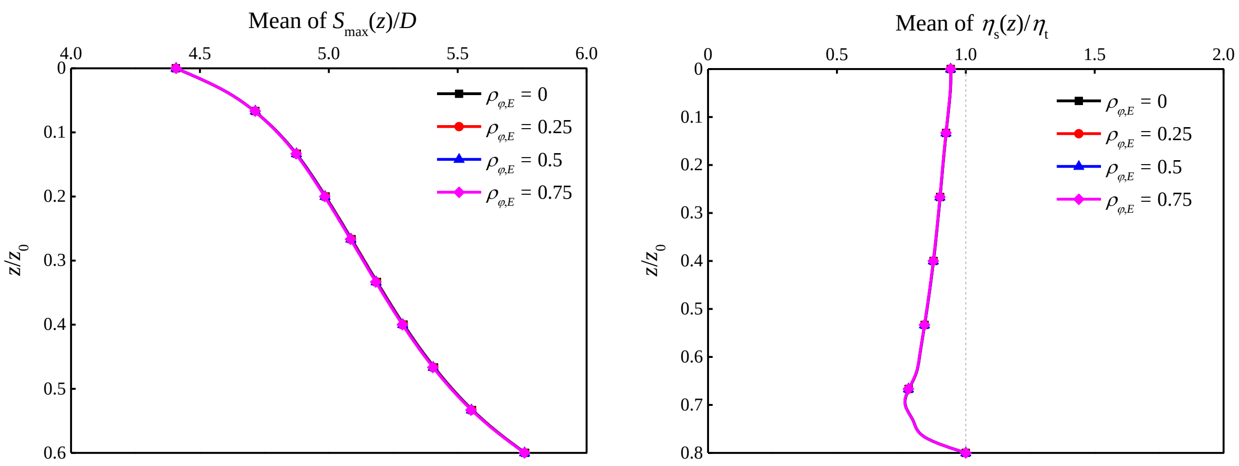

(a) (b)

Fig. S8 Mean of stochastic analysis results under different $\rho_{\varphi,E}$: (a) Normalized subsurface maximum settlement; (b) Normalized subsurface soil volume loss rate

References

Wang, F., Du, X., Li, P., 2024. Prediction of subsurface settlement induced by shield tunnelling in sandy cobble stratum. *Journal of Rock Mechanics and Geotechnical Engineering*, 16: 192–212. https://doi.org/10.1016/j.jrmge.2023.08.001

Du, X., Zhang, P., Jin, L., et al., 2019. A multi-scale analysis method for the simulation of tunnel excavation in sandy cobble stratum. Tunnelling and Underground Space Technology, 83: 220–230. https://doi.org/10.1016/j.tust.2018.09.019

Schanz, T., Vermeer, P.A., Bonnier, P.G., 1999. The hardening soil model: Formulation and verification. Beyond 2000 in computational geotechnics. Ten Years of PLAXIS International. Proceedings of the international symposium, Amsterdam, p. 281–296. https://doi.org/10.1201/9781315138206-27

Huang, S.P., Quek, S.T., Phoon, K.K., 2001. Convergence study of the truncated Karhunen–Loeve expansion for simulation of stochastic processes. International Journal for Numerical Methods in Engineering, 52: 1029–1043. https://doi.org/10.1002/nme.255

Laloy, E., Rogiers, B., Vrugt, J.A., et al., 2013. Efficient posterior exploration of a high-dimensional groundwater model from two-stage Markov chain Monte Carlo simulation and polynomial chaos expansion. Water Resource Research, 49: 2664–2682. https://doi.org/10.1002/wrcr.20226

Jiang, S.H., Li, D.Q., Zhang, L.M., et al., 2014. Slope reliability analysis considering spatially variable shear strength parameters using a non-intrusive stochastic finite element method. Engineering Geology, 168: 120–128. https://doi.org/10.1016/j.enggeo.2013.11.006